Draft version June 8, 2022
Typeset using LaTeX **twocolumn** style in AASTeX631

A convenient, flexible and intuitive analytic expression for the metallicity-dependent cosmic star formation rate

L. A. C. van Son,[1,2,3] S. E. de Mink,[3,2,1] R. Pakmor,[3] and et al?

[1] *Center for Astrophysics | Harvard & Smithsonian, 60 Garden St., Cambridge, MA 02138, USA*
[2] *Anton Pannekoek Institute of Astronomy and GRAPPA, Science Park 904, University of Amsterdam, 1098XH Amsterdam, The Netherlands*
[3] *Max Planck Institute for Astrophysics, Karl-Schwarzschild-Str. 1, 85748 Garching, Germany*

ABSTRACT

New observational facilities are probing star formation and stellar transients and gravitational wave sources at ever increasing redshifts. Comparing these observations with predictions from model for stellar populations or the channels for the formation of gravitational wave sources require assumptions for the cosmic starformation rate density and, in particular, how this depends on metallicity. Various approaches exist ranging from fully empirical prescriptions to prescriptions that are based on cosmological simulations. Both these approaches come with advantages and disadvantages and inherent uncertainties.

To make it easier to produce model predictions we propose a simple analytical prescription that captures the main behavior of the advanced simulations. At the same time, the prescription comes with parameters that allow for variations in the overall shape and which can be easily interpreted. Our hope is that this expression provides a useful starting point for making predictions and comparison with observations.

1. INTRODUCTION

LIGO/Virgo are revealing double compact object mergers throughout the Universe. These systems originate from largely

Since the delay time of BBHs can range from Myrs to multiple Gyrs, the birth environment of BBHs varies significantly and we cannot ignore the cosmological (metallicity) evolution of the Universe. The rate of Binary Black Hole (BBH) mergers at different redshifts depends both on the delay time distribution as well as the metallicity dependent star-formation rate density ($\mathcal{S}(Z, z)$). The assumed cosmic star formation rate density (SFRD) will therefore greatly influence the observed rate of double compact object mergers (Neijssel et al. 2019a; **?**; Boco et al. 2020; Broekgaarden et al. 2021a). Moreover, it is the nuclear reactions in massive stars are responsible for the metal enrichment of the Universe at high redshift. The birth of massive stars, and their death as BHs are thus inseparable from the evolution of the metallicity distribution of the Universe.

Corresponding author: L. van Son
lieke.van.son@cfa.harvard.edu

Merging BBHs are found to form more efficiently at low metallicities e.g. (e.g. Belczynski et al. 2010; Stevenson et al. 2017; Mapelli et al. 2017a; Chruślińska et al. 2019). Therefore the assumed metallicity specific star formation rate will in particular have a large impact on the inferred merger rate (e.g. Chruślińska & Nelemans 2019; Chruślińska et al. 2019; Neijssel et al. 2019b; Broekgaarden et al. 2021a).

It is difficult to observationally constrain the shape of the metallicity density distribution over redshift (see Chruślińska & Nelemans (2019) for an extensive overview and discussion of relevant observational caveats). Traditionally the metallicity density distribution is estimated by combining a mass-metallicity relation (MZ-relation) and a galaxy stellar mass function (GSMF) (see also Chruslinska et al. 2018; Chruślińska et al. 2019; Broekgaarden et al. 2021a). Another way is to extract the metallicity density fraction from cosmological simulations (Mapelli et al. 2017a; Schneider et al. 2017, e.g.) Alternatively, one can combine an observed star formation rate, SFR(z), like from Madau & Dickinson (2014) or Madau & Fragos (2017), and convolve this with some belief about the shape of the metallicity density distribution, such as was was done in Neijssel et al. (2019a). A third option is extract this informa-

tion from cosmological simulations (e.g. Mapelli et al. 2017b; Schneider et al. 2017). In this work we provide a new fit to the $\mathcal{S}(Z,z)$ based on the TNG 100 simulation (Pillepich et al. 2018a; Weinberger et al. 2017).

Large uncertainties exist in the shape and redshift evolution of both SFRD(z), and dP/dZ(Z,z) (see e.g. Chruślińska & Nelemans 2019, Boco et al. 2021 and Chruślińska et al. 2021 for an extended discussion on the metallicity dependent star formation rate density, in light of empirical data).

To construct $\mathcal{S}(Z,z)$ from empirical data, one can estimate dP/dZ(Z,z) by combining observed mass-metallicity relations with galaxy stellar mass functions (see e.g. Chruslinska et al. 2018; **?**; Broekgaarden et al. 2021b). Alternatively, one could extract $\mathcal{S}(Z,z)$ directly from cosmological simulations (e.g. Mapelli et al. 2017a; Briel et al. 2021).

In this work, we take an approach similar to Mapelli et al. (2017a) and Briel et al. (2021) but instead of directly extracting the $\mathcal{S}(Z,z)$ from a cosmological simulation we fit analytical representations of SFRD(z) and dP/dZ(Z,z) to simulation data.

By adopting an analytical, parametrized form for $\mathcal{S}(Z,z)$, the large uncertainties in $\mathcal{S}(Z,z)$ can be systematically explored through smoothly varying the parameters that control its shape (cf. Briel et al. 2021).

Different cosmological simulations produce varying $\mathcal{S}(Z,z)$ which lead to different redshift evolution of the BBH merger rate with redshift. Briel et al. (2021) find that the EAGLE and TNG simulation provide the best $\mathcal{S}(Z,z)$ based on the predicted cosmic rates for electromagnetic and gravitational-wave transients. Although we only consider our fit to describe the IllustrisTNG100 simulation and the phenomenological fit from Neijssel et al. (2019a), our prescription can be easily be updated to fit other observational or simulated data of the metallicity dependent star formation rate density.

2. ILLUSTRIS-TNG COSMOLOGICAL SIMULATIONS

The IllustrisTNG-project considers galaxy formation and evolution through large-scale cosmological hydrodynamical simulations.

Insert a description of enrichment and gas recycling.

They have been shown to reproduce many of the global properties of galaxies and their scaling relations for a representative portion of the Universe (e.g. Naiman et al. 2018; Torrey et al. 2019; Genel et al. 2018; Hemler et al. 2021).These simulations are publicly available[1] (Springel et al. 2018; Marinacci et al. 2018; Nelson et al. 2018; Pillepich et al. 2018b; Naiman et al. 2018).

3. A CONVENIENT ANALYTIC EXPRESSION FOR THE METALLICITY-DEPENDENT STAR FORMATION RATE DENSITY

We assume that the metallicity dependent star formation rate density can be separated into two independent functions (e.g. Langer & Norman 2006),

$$\mathcal{S}(Z,z) = \mathrm{SFRD}(z) \times \frac{\mathrm{dP}}{\mathrm{dZ}}(Z,z). \tag{1}$$

The first term is the star formation rate density, SFRD(z), that is the amount of mass formed in stars per unit time and per unit comoving volume at each redshift. The second term, dP/dZ(Z,z), is a probability density function that expresses what fraction of star formation occurs at which metallicity, at each redshift.

3.1. *The metallicity probability density function*

For the probability distribution of metallicities we draw inspiration from the approach by (e.g. Neijssel et al. 2019a) who used a log-normal distribution. Unfortunately, this expression does not capture the asymmetry well that we see in the results of the cosmological simulations, which show an extended tail towards low metallicity combined with a very limited tail towards higher metallicity, when plotted as a function of $\log_1 0Z$. To capture this behavior we adopt a skewed-log-normal distribution instead. This is an extension of the normal distribution that introduces an additional shape parameter, α, that regulates the skewness (O'Hagan & Leonard 1976). This allows us to more accurately capture the asymmetry in the metallicity distribution at each redshift.

The skewed-log-normal distribution of metallicities is defined as:

$$\begin{aligned}\frac{\mathrm{dP}}{\mathrm{dZ}}(Z) &= \frac{1}{Z} \times \frac{\mathrm{dP}}{\mathrm{d}\ln Z} \\ &= \frac{2}{Z} \times \underbrace{\phi\left(\frac{\ln Z - \xi}{\omega}\right)}_{(1)} \underbrace{\Phi\left(\alpha\frac{\ln Z - \xi}{\omega}\right)}_{(2)},\end{aligned} \tag{2}$$

where (1) is the standard log-normal distribution, ϕ,

$$\phi\left(\frac{\ln Z - \xi}{\omega}\right) \equiv \frac{1}{\omega\sqrt{2\pi}} \exp\left\{-\frac{1}{2}\left(\frac{\ln Z - \xi}{\omega}\right)^2\right\} \tag{3}$$

[1] https://www.tng-project.org/

and (2) is the new term that allows for asymmetry, which is equal to the cumulative of the log-normal distribution, Φ,

$$\begin{aligned}\Phi\left(\alpha\tfrac{\ln Z-\xi}{\omega}\right) &\equiv \tfrac{1}{2}\left(1+\operatorname{erf}\left\{\alpha\tfrac{\ln Z-\xi}{\omega\sqrt{2}}\right\}\right)\\ &= \tfrac{1}{2}\int_{\infty}^{\alpha\left(\frac{\ln Z-\xi}{\omega}\right)}\tfrac{1}{\sqrt{2\pi}}e^{-t^2/2}dt\end{aligned} \tag{4}$$

This introduces three parameters, α, ω and ξ each of which may depend on redshift. The first parameter, α, is known as the "shape". It affects the skewness of the distribution and thus allows for asymmetries between metallicities that are higher and lower than the mean. The symmetric log-normal distribution is recovered for $\alpha = 0$. The second parameter, ω is known as the "scale". It provides a measure of the spread in metallicities at each redshift. Finally, ξ, is known as the "location", because this parameter plays a role in setting the mean of the distribution at each redshift.

The location and the mean of the metallicity distribution— To obtain a useful expression for the redshift dependence of the "location" $\xi(z)$ we first express the expectation value or mean metallicity at a given redshift

$$\langle Z\rangle = 2\exp\left(\frac{\xi\,\omega^2}{2}\right)\Phi\left(\beta\,\omega\right) \tag{5}$$

where β is

$$\beta = \frac{\alpha}{\sqrt{1+\alpha^2}}. \tag{6}$$

For the evolution of the mean metallicity with redshift we follow Neijssel et al. (2019a) and Langer & Norman (2006) in assuming that the mean of the probability density function of metallicities evolves with redshift as:

$$\langle Z\rangle \equiv \mu(z) = \mu_0\cdot 10^{\mu_z\cdot z}, \tag{7}$$

where μ_0 is the mean metallicity at redshift 0, and μ_z determines redshift evolution of the location. Equating this to Equation 5, we get an expression for $\xi(z)$,

$$\xi(z) = -\frac{\omega^2}{2}\,\ln\left(\frac{\mu_0\cdot 10^{\mu_z\cdot z}}{2\,\Phi(\beta\,\omega)}\right). \tag{8}$$

The scale (and variance) of the metallicity distribution—We will also allow the "scale" w also evolves with redshift in a similar manner,

$$\omega(z) = \omega_0\cdot 10^{\omega_z\cdot z}. \tag{9}$$

where ω_0 is the width of the metallicity distribution at $z = 0$, and ω_z the redshift evolution of the scale.

Note that the width, $w(z)$ is not the same as the variance. The variance, $\sigma(z)^2$, can be expressed as

$$\sigma(z)^2 = \omega(z)^2\left(1-\frac{2\beta^2}{\pi}\right) \tag{10}$$

Assymetry of the metallicity distribution: α—We have considered variations where the "skewness" α varies with redshift but we did not find very significant improvements compared to the simpler assumption where α is kept constant.

In summary, Equation 2 becomes:

$$\frac{\mathrm{dP}}{\mathrm{dZ}}(Z,z) = \frac{2}{Z}\times\phi\left(\frac{\ln Z-\xi(z)}{\omega(z)}\right)\Phi\left(\alpha\frac{\ln Z-\xi(z)}{\omega(z)}\right), \tag{11}$$

where $\xi(z)$ and $\omega(z)$ are defined in Equations 8 and 9 respectively and we have assumed α to be constant.

3.2. *The overall cosmic star formation rate density*

For the star formation rate density, we assume the analytical form proposed by Madau & Dickinson (2014),

$$\mathrm{SFRD}(z) = \frac{d^2M_{\mathrm{SFR}}}{dtdV_c}(z) = a\frac{(1+z)^b}{1+[(1+z)/c]^d} \tag{12}$$

in units of $\left[\mathrm{M}_\odot\,\mathrm{yr}^{-1}\,\mathrm{cMpc}^{-3}\right]$. This introduces four parameters, a which sets the overal normalisation and which has the same units as $\mathrm{SFRD}(z)$ and b, c and d which are unitless and which govern the shape of the overal cosmic starformation rate density with redshift.

3.3. *Combined function*

We combine equations 11 and 12 to form a full metallicity specific starformation rate density ($\mathcal{S}(Z,z)$). We fit for the following nine free parameters $\alpha, \mu_0, \mu_z, \omega_0, \omega_z$, which govern the metallicity dependence and a, b, c and d, which set the overall starformation rate.

4. ANALYTICAL FIT AGAINST COSMOLOGICAL SIMULATION

The task we have at hand here is not a standard textbook fitting problem given the specific aims and requirements that we have that are driven by the astrophysical applications we have in mind. Qualitatively, our aims are the following. Our main aim is to find solution for the free parameters, for which the expression reproduces the overall behaviour that is observed in the cosmological simulations. For the purposes we have in mind, it will be more important to prioritise fitting the large scale trends, while we are not so interested in smaller scale fluctuations. We further prioritise getting the bulk of the cosmic star formation right and are less interested in capturing the behaviour in metallicity and redshift bins where the cosmic starformation rate is very low and thus insignificant for the overall picture. Finally, we are especially interested in capturing the asymmetry of the metallicity distribution.

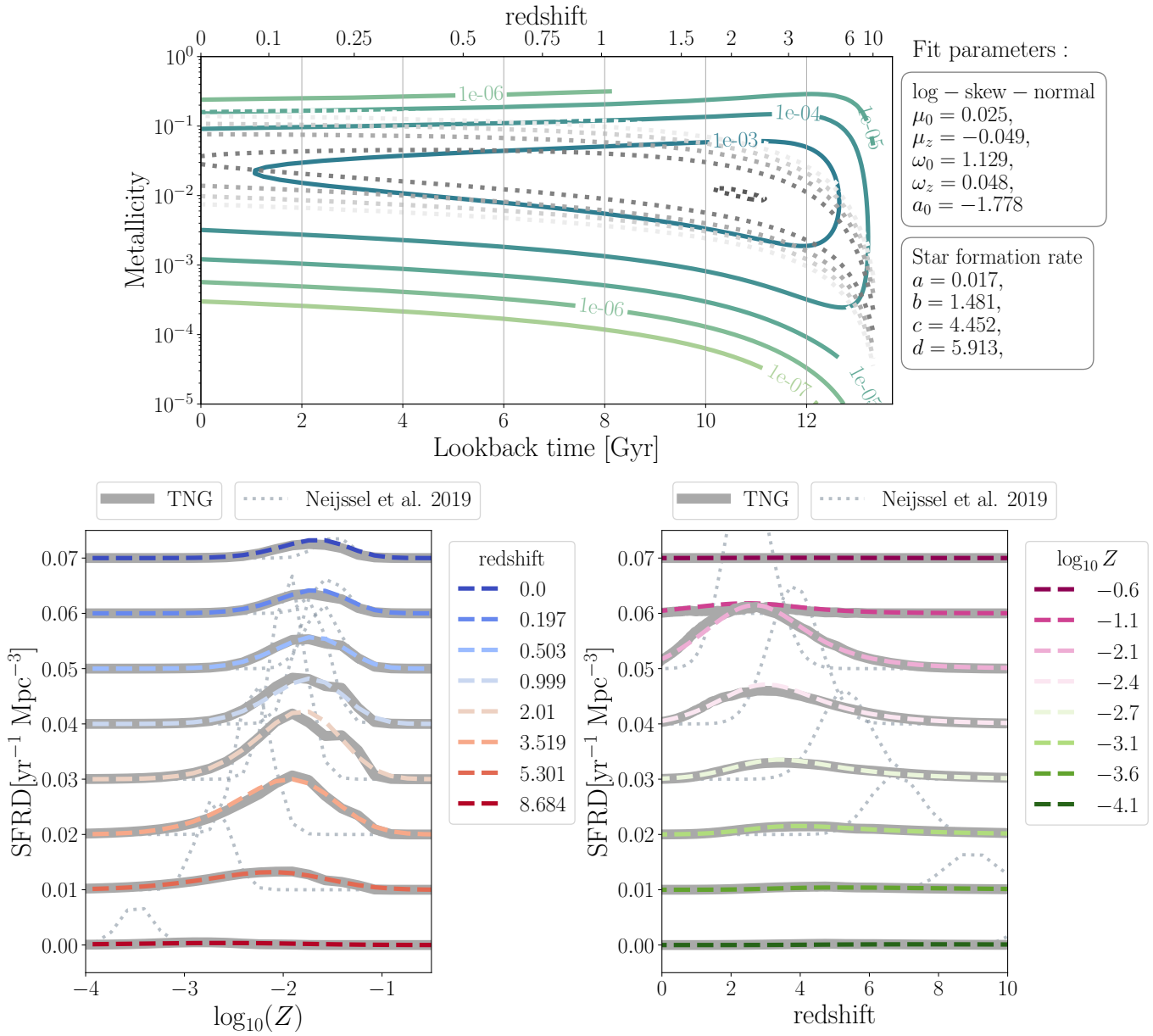

Figure 1. Fit for SFRD shown against TNG and Neijssel.

There is not one unique procedure that will full fill these criteria. After experimenting with different criteria we have adopted the procedure below, which we believe works well for the aims we have in mind.

4.1. *Choices and binning of the data*

We fit our function to the metallicity distribution of the starforming gas in the TNG100 simulation. For this we use a binned version of the TNG data $\mathcal{S}(Z, z)_{\rm sim}$. We consider metallicities between $Z = -5$ to $\log_{10} Z = 0$ in 30 bins, where we use Z_i to refer to the logarithmic centers of the bins. We ignore star formation in metallicities $\log_{10} Z \leq -5$ as this only accounts for less than 1% of the total cosmic starformation rate in these simulations.

We consider bins in redshifts between $z = 0$ and $z = 10$, with a step size of $dz = 0.05$, where z_j refers to the centers of the bins.

4.2. *Optimisation function*

To find a solution we use a method based on the sum of the quadratic differences between the simulations and our fit function. Using a vanilla χ-squared approach does not serve our purposes very well as it does a poor job in fitting regions where the starformation is very low. Using a χ-squared approach on the logarithm of the function instead places far too much weight on trying to fit the starformation rate in regions where the rate is very low or not even significant. After experimenting,

Table 1. Best fitting parameters for our $\mathcal{S}(Z, z)$ fit to TNG100 data.

dP/dZ param.	best fit	SFRD(z) param.	best fit
μ_0	0.025	a	0.02
μ_z	-0.048	b	1.48
α_0	-1.767	c	4.45
ω_0	1.125	d	5.90
ω_z	0.048		

we find that the following approach gives us satisfactory results.

We first consider a given redshift z_j. For this redshift we compute the sum of the squared residuals between the cosmological simulation and our fit.

$$\chi^2(z_j) \equiv \sum_{Z_i} \left(\mathcal{S}(Z_i, z_j)_{\rm sim} - \mathcal{S}(Z_i, z_j)_{\rm fit}\right)^2 \qquad (13)$$

Here, the variable Z_i runs over all redshift bins, but excludes bins where the starformation rate density is lower $10^{-10}\mathrm{M}_\odot\,\mathrm{yr}\,\mathrm{Gpc}^{-3}$ per bin.

Subsequently we sum the $\chi^2(z_j)$ for all redshift bins z_j. To ensure that our fit procedure gives sufficient weight to the behaviour at all redshifts, we find that we need to introduce a penalisation factor to somewhat reduce the contribution of redshifts where the peak of cosmic starformation occurs, while increasing the weight where at redshifts where the overal cosmic starformation rate is lower. To achieve this we divide $\chi^2(z_j)$ by the starformation $\sum_{Z_i}\mathcal{S}(Z_i, z_j)$ per redshift bin before adding the contribution of all redshifts. Our final expression for the cost function reads

$$\chi = \sum_{z_j} \frac{\chi^2(z_j)}{\sum_{Z_i}\mathcal{S}(Z_i, z_j)} \qquad (14)$$

We use the `scipy.optimize.minimize` from SciPy v1.6.3 implementation of the optimized quasi-Newton method of Broyden, Fletcher, Goldfarb, and Shanno (BFGS) http://www.apmath.spbu.ru/cnsa/pdf/monograf/Numerical_Optimization2006.pdf

With the fit parameters as mentioned above, we find a maximum residual between the model and the TNG100 data of $2.3 \cdot 10^{-3}\mathrm{M}_\odot\,\mathrm{yr}^{-1}\,\mathrm{Gpc}^{-3}$ at any given redshift.

Our best fitting parameters are listed in Table 1. With these fit parameters, $\chi^2(z_j)$ is smaller than $2 \cdot 10^{-4}$ at any given redshift.

5. EFFECT ON THE LOCAL MASS DISTRIBUTION OF BBH MERGERS

REFERENCES

Belczynski, K., Bulik, T., Fryer, C. L., et al. 2010, ApJ, 714, 1217, doi: 10.1088/0004-637X/714/2/1217

Boco, L., Lapi, A., Chruslinska, M., et al. 2020, arXiv e-prints, arXiv:2012.02800. https://arxiv.org/abs/2012.02800

Boco, L., Lapi, A., Chruślińska, M., et al. 2021, ApJ, 907, 110, doi: 10.3847/1538-4357/abd3a0

Briel, M. M., Eldridge, J. J., Stanway, E. R., Stevance, H. F., & Chrimes, A. A. 2021, arXiv e-prints, arXiv:2111.08124. https://arxiv.org/abs/2111.08124

Broekgaarden, F. S., Berger, E., Neijssel, C. J., et al. 2021a, arXiv e-prints, arXiv:2103.02608. https://arxiv.org/abs/2103.02608

Broekgaarden, F. S., Berger, E., Stevenson, S., et al. 2021b, arXiv e-prints, arXiv:2112.05763. https://arxiv.org/abs/2112.05763

Chruslinska, M., Belczynski, K., Klencki, J., & Benacquista, M. 2018, MNRAS, 474, 2937, doi: 10.1093/mnras/stx2923

Chruślińska, M., & Nelemans, G. 2019, MNRAS, 488, 5300, doi: 10.1093/mnras/stz2057

Chruślińska, M., Nelemans, G., & Belczynski, K. 2019, MNRAS, 482, 5012, doi: 10.1093/mnras/sty3087

Chruślińska, M., Nelemans, G., Boco, L., & Lapi, A. 2021, MNRAS, 508, 4994, doi: 10.1093/mnras/stab2690

Genel, S., Nelson, D., Pillepich, A., et al. 2018, MNRAS, 474, 3976, doi: 10.1093/mnras/stx3078

Hemler, Z. S., Torrey, P., Qi, J., et al. 2021, MNRAS, 506, 3024, doi: 10.1093/mnras/stab1803

Langer, N., & Norman, C. A. 2006, ApJL, 638, L63, doi: 10.1086/500363

Madau, P., & Dickinson, M. 2014, ARA&A, 52, 415, doi: 10.1146/annurev-astro-081811-125615

Madau, P., & Fragos, T. 2017, ApJ, 840, 39, doi: 10.3847/1538-4357/aa6af9

Mapelli, M., Giacobbo, N., Ripamonti, E., & Spera, M. 2017a, MNRAS, 472, 2422, doi: 10.1093/mnras/stx2123

—. 2017b, MNRAS, 472, 2422, doi: 10.1093/mnras/stx2123

Marinacci, F., Vogelsberger, M., Pakmor, R., et al. 2018, MNRAS, 480, 5113, doi: 10.1093/mnras/sty2206

Naiman, J. P., Pillepich, A., Springel, V., et al. 2018, MNRAS, 477, 1206, doi: 10.1093/mnras/sty618

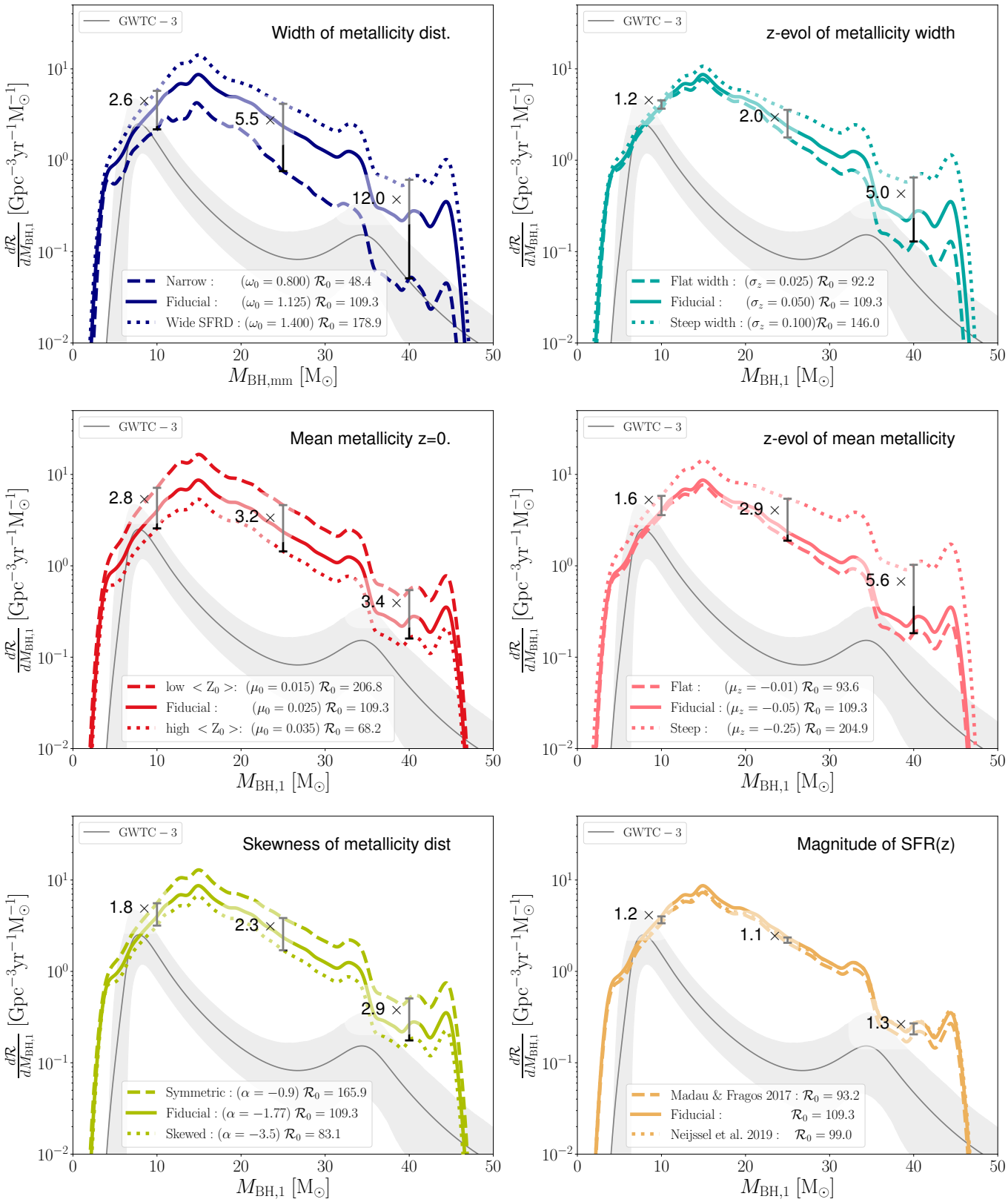

Figure 2. The effects of several variations in the SFRD

Neijssel, C. J., Vigna-Gómez, A., Stevenson, S., et al. 2019a, MNRAS, 2457, doi: 10.1093/mnras/stz2840

—. 2019b, MNRAS, 490, 3740, doi: 10.1093/mnras/stz2840

Nelson, D., Pillepich, A., Springel, V., et al. 2018, MNRAS, 475, 624, doi: 10.1093/mnras/stx3040

O'Hagan, A., & Leonard, T. 1976, Biometrika, 63, 201, doi: 10.1093/biomet/63.1.201

Pillepich, A., Springel, V., Nelson, D., et al. 2018a, MNRAS, 473, 4077, doi: 10.1093/mnras/stx2656

Pillepich, A., Nelson, D., Hernquist, L., et al. 2018b, MNRAS, 475, 648, doi: 10.1093/mnras/stx3112

Schneider, F. R. N., Castro, N., Fossati, L., Langer, N., & de Koter, A. 2017, A&A, 598, A60, doi: 10.1051/0004-6361/201628409

Springel, V., Pakmor, R., Pillepich, A., et al. 2018, MNRAS, 475, 676, doi: 10.1093/mnras/stx3304

Stevenson, S., Vigna-Gómez, A., Mandel, I., et al. 2017, Nature Communications, 8, 14906, doi: 10.1038/ncomms14906

Torrey, P., Vogelsberger, M., Marinacci, F., et al. 2019, MNRAS, 484, 5587, doi: 10.1093/mnras/stz243

Weinberger, R., Springel, V., Hernquist, L., et al. 2017, MNRAS, 465, 3291, doi: 10.1093/mnras/stw2944